Spatiotemporal Resonances in Mixing of Open Viscous Fluids

F. Okkels[1,2] and P. Tabeling[1]

[1]*Microfluidique, MEMS, Nanostructures, ESPCI, 10 rue Vauquelin, 75005 Paris, France*
[2]*MIC Micro- and Nanotechnology Research Institute, DTU, 2800 Lyngby, Denmark*

(Received 5 May 2003; published 22 January 2004)

In this Letter, we reveal a new dynamical phenomenon, called "spatiotemporal resonance," which is expected to take place in a broad range of viscous, periodically forced, open systems. The observation originates from a numerical and theoretical analysis of a micromixer, and is supported by preliminary experimental observations. The theoretical model nicely matches the numerical results, which again is supported by the experiment. Because of the general nature of the phenomenon, this phenomenon is not limited to microsystems. Because of the resonances, a slight tuning of the control parameters makes the mixer enhance the mixing, or suppress it, enhancing interfacial diffusion instead.

DOI: 10.1103/PhysRevLett.92.038301 PACS numbers: 83.50.Xa, 76.20.+q, 05.45.–a, 85.85.+j

Mixing of fluids on a microscale is a nontrivial problem: The reason is that microfluid flows are governed by low or extremely low Reynolds numbers, ruling out hydrodynamic instabilities and turbulence. As a consequence, diffusion plays a dominant role and, in practice, this leads to long mixing times often incompatible with the expectation that miniaturization favors fast dynamics [1]. Nonchaotic mixers, taking advantage of Taylor-Aris (axial) dispersion enhancement, have been proposed [2], but faster mixing rates can be expected using the idea of *laminar mixing* or *chaotic advection*, developed by several groups [3,4].

This Letter concerns the numerical and theoretical analysis of a simple micromixer [5] from now on called "the mixer." It produces an active mixing since the flow field comes from an external source [6–8], in contrast to passive mixing, where the flow field is produced intrinsically due to the detailed geometry of the channel [9,10].

The resonance phenomenon presented here depends on a few necessary conditions in which the flow geometry and forcing have to fulfill some spatial and temporal symmetries and the flow has to be creeping, i.e., viscosity dominated. As none of these conditions are restricted to microfluidics, we assume that these resonances may be of interest to the whole fluid-dynamical society and not just to the field of microfluidics.

The purpose of the present Letter is twofold: both to give the theoretical basis for working with and developing active mixers and to report on the discovery of "spatiotemporal resonance," which to the best of our knowledge has not been noticed before.

The mixer consists of two microchannels of width L meeting in a cross, as shown in Fig. 1. Here, a main steady flow of velocity V and consisting of two fluid layers approaches the cross from the left channel, forming a straight interface between the fluids. Without any transverse flow, the interface will continue unaffected through the cross, but once a transverse flow is established it perturbs the shape of the interface. In the case we consider, the transverse flow changes periodically in time, modulated by the oscillating function: $f(t) = A\cos\omega t$ with amplitude velocity A and angular velocity ω.

Because of the very low Reynolds numbers, we work with creeping flows, and the flow problem in the mixer becomes linear. This makes it possible to get the periodic flow field by superimposing a constant mean flow of velocity V with a periodical transverse flow of velocity $A\cos\omega t$.

In the experimental setup, we use wide narrow channels, which is best modeled by a three-dimensional (3D) creeping flow, but in order to cope with the theoretical and numerical work, we restrict the model to two-dimensional (2D) creeping flow, in reality corresponding to infinitely deep channels, which give rise to parabolic velocity profiles across straight channels. Despite this difference between model and experiment, we observe a nice agreement, as shown later.

With these assumptions and introducing the following nondimensional control parameters,

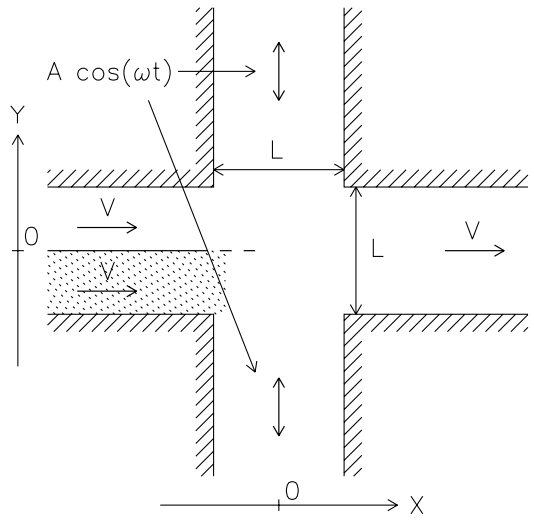

FIG. 1. Schematic setup of the mixer with the characteristic quantities and axes.

$$\alpha = \frac{A}{V}, \qquad \Omega = \omega \frac{\mathrm{L}}{V}, \tag{1}$$

one obtains the dimensionless governing equations for the mixer in the following form:

$$d\vec{X}/dt = \vec{V}_M + f(t) \cdot \vec{V}_T, \qquad f(t) = \alpha \cos\Omega t, \tag{2}$$

where $\vec{V}_M(\vec{V}_T)$ corresponds to pure main (transverse) flows with maximal velocity equal to unity in channels of unit width. We let these equations, which describe simple passive advection, completely determine the state and dynamics of the mixer.

Generally assuming a no-slip condition at the channel wall boundaries and open flow at the channel inlets/outlets, the 2D creeping flow gives rise to a parabolic velocity profile far from the cross junction, but in order to obtain the nontrivial flow field at the junction we solve the full 2D Navier-Stokes equations in the geometry of Fig. 1 for very low Reynolds numbers [11]. All computations were done on a single Apple PowerBook G4 using IDL [13] both for simulation and presentation.

To describe the interface dynamics from the full time-varying flow field, we numerically calculate the deformation of a material line (demarcation line) entering the cross section. This is done by releasing a dense string of interface points, at a constant rate, from a fixed position far upstream at the middle of the left channel, and advecting them passively by the flow, using linear interpolation to calculate subgrid velocities.

From inspection of the results, we observe the general behavior that the folding increases as the amplitude α increases and the angular velocity Ω decreases. Figure 2 shows a collection of snapshots of the interface across the mixer for different control parameters, where 2(a) shows very weak perturbation of the interface as $\Omega > \alpha$, while violent folding is shown in 2(b) with $\Omega < \alpha$. Beside this common trend, strong variation in folding can occur within a small region of the control-parameter space as shown in 2(c)–2(e): The state of poor folding 2(d) exists in between states of better folding 2(c) and 2(e).

This indicates a more complex dependence on the control parameters, which will be the concern of the rest of the Letter. It will turn out that bands of poor folding enter into regions of otherwise strong folding, and we will denote these band *resonances* as justified later.

In order to investigate the resonances more thoroughly, we make a detailed scan of the parameter space, where the folding of each state is quantified. To construct such a quantity we note the following.

First, because of the periodic nature of the problem, we only need to analyze an interface segment released during one forcing period. Second, we compensate for the continuous distortion of the interface segment due to the parabolic velocity profile before further analysis.

A quantity strongly related to the amount of folding of a segment is its arclength, denoted L_a, which is normalized by the length of a reference curve of similar size. Letting the horizontal (vertical) extend of the segment be $dx(dy)$, and looking for the shortest periodic curve bounded by dx, dy, we end up using a sawtooth curve for reference, as shown in Fig. 3. Denoting the arclength of the reference curve L_r, we define the folding quantity:

$$F = \frac{L_a}{L_r} - 1, \qquad \text{with } L_r = \sqrt{dx^2 + 4\,dy^2}. \tag{3}$$

With no perturbation the interface segment becomes a horizontal line, making $F = 0$ and from there increasing with the complexity of the folding [14].

The folding quantity F has been mapped through a region of the parameter space and is shown as a contour plot in Fig. 4 with contours increasing in logarithmic steps,

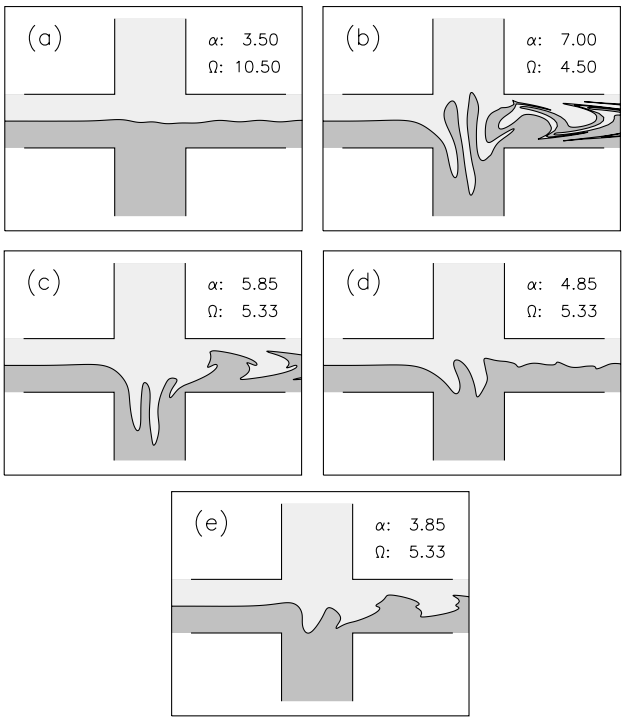

FIG. 2. Example of interface snapshots for different control parameters: (a)/(b), poor/strong mixing; (c)–(e), strong local variations in mixing efficiency.

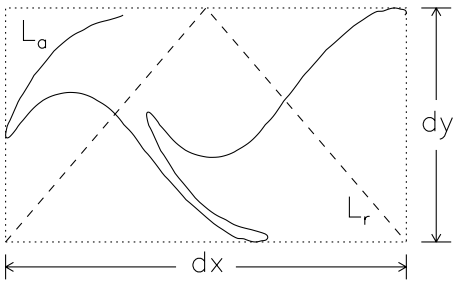

FIG. 3. Illustration of how to define the folding quantity F. Solid curve is the interface segment; dashed curve is the reference curve, and dx, dy denotes their extend.

filled with a darkening gray scale proportional to $\log F$ for $10^{-3} \leq F \leq \approx 4.64$. In Fig. 4, one clearly sees resonances (light) penetrating into regions of good mixing (dark), and the five squares correspond to the interfaces shown in Fig. 2, which confirms the poor mixing seen in Fig. 2(d) as it is positioned on a resonance. In Fig. 4, it should be emphasized that $F = 0$ on the line $\alpha = 0$.

It turns out that the resonances can be explained and modeled using general properties of the mixer.

The nature of the resonances is explained as follows: A resonance of inefficient mixing occurs when the perturbation of a point on the interface during the first half of the mixing region is completely reversed during the last part, resulting in vanishing net perturbation.

A necessary condition in order to obtain resonances is a y symmetry of the flow geometry at the crossing, and a 2π-periodic forcing function $f(\phi)$, which is odd at $\phi = \pi/2$: $f[-(\phi - \pi/2)] = -f(\phi - \pi/2)$. With these conditions, the resonances depend only on the two natural time scales of the mixer, which are needed to reverse the forcing at the middle of the channel: the period of the forcing $T_P = 2\pi/\Omega$, and the advection time T_A of a point on the interface through the active mixing region.

The explanation of the resonances gives the following relation between the characteristic time scales:

$$T_A = C_n T_P, \qquad \text{where } C_n = n + \tfrac{1}{2}, \qquad n \in \mathbb{N}, \quad (4)$$

where C_n comes as the perturbation has to change an odd number of half phases during the passing of the interface point: $C_n = (2n + 1)/2 = n + \frac{1}{2}$.

Equation (4) has been justified numerically by computing trajectories of interface points, and it also justifies the term "resonance" as it relates two time scales. It further shows that the main theoretical goal is to estimate T_A as a function of the forcing parameters Ω, α, as done in the following.

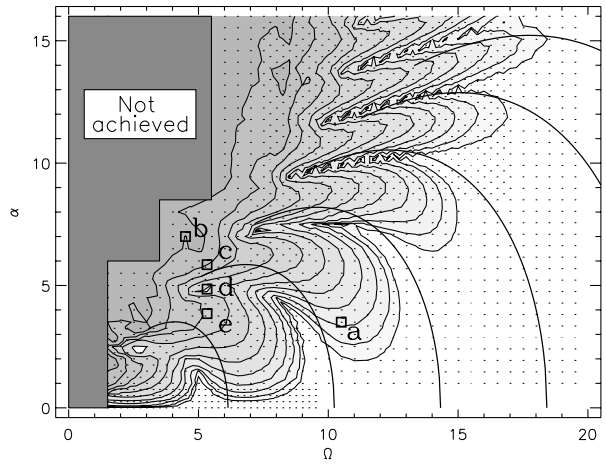

FIG. 4. Contour plot of the folding quantity F as a function of the control parameters Ω, α. Points for each measurement of F; squares for states shown in Fig. 2; solid curves for theoretical resonances predicted by Eq. (9).

We begin by modeling a simplified flow field using Eq. (2) and, when neglecting the small side-way contributions to the pure velocity fields, we separate the advection into coordinates [$\vec{V}_M = (V_{M,x}, V_{M,y})$ etc.]:

$$\frac{dx}{dt} = V_{M,x}(y), \qquad \frac{dy}{dt} = f(t)\, V_{T,y}(x). \quad (5)$$

From the initial condition $y(0) \equiv 0$, and assuming slow variations of $x(t)$ compared to $y(t)$, we get $y(x, t) = V_{T,y}(x)\, F(t)$, $F(t) = \frac{\alpha}{\Omega} \sin\Omega t$, and when inserted into the first part of Eq. (5) we get the dynamics of x:

$$\frac{dx}{dt} = V_{M,x}(y) = V_{M,x}[V_{T,y}(x) F(t)], \quad (6)$$

which will be used to determine T_A. Even though the assumption of a slowly varying $x(t)$ holds for high α, numerical integrations of Eqs. (5) and (6) show similar dynamics of $x(t)$ even for small α, which remains a puzzle to the authors.

In the main channel the parabolic velocity profile is given simply by $V_{M,x}(y) = 1 - 4y^2$, but at the crossing the flow broadens and we introduce profiles rescaled by a width factor b, ($b > 1$):

$$V_{M,x}(y) = \frac{1}{b}\left(1 - \frac{4y^2}{b^2}\right), \qquad V_{T,y}(x) = \frac{1}{b}\left(1 - \frac{4x^2}{b^2}\right). \quad (7)$$

The width factor also defines the active mixing region which extends $b/2$ into both channels from the center of the crossing, giving the initial condition for the solution of Eq. (6): $[x(0), y(0)] \equiv [-b/2, 0]$.

Inserting Eq. (7) into Eq. (6), we approximate $[1 - (4x^2)/b^2]^2$ with a constant function of equal integral in the range of $x \in [-b/2, b/2]$, and thereby having the constant value of $\Gamma = 8/15$. The evolution of x now becomes

$$x(t) = \frac{t}{b}\left(1 - \frac{2\Gamma\alpha^2}{b^4\Omega^2}\right) + \frac{\Gamma\alpha^2}{b^5\Omega^3} \sin 2\Omega t - b/2. \quad (8)$$

Because of the resonances relation given by Eq. (4), an interface point has to pass through the active mixing region in a specific time ($T_A = C_n T_P$) and this gives the resonance condition on $x(t)$: $x(C_n T_P) \equiv b/2, n \in \mathbb{N}$. Inserting this into Eq. (8), we finally get the relation between α and Ω in order for resonances to occur:

$$\alpha = b^2\Omega \sqrt{\frac{15}{16}\left(1 - \frac{b^2\Omega}{2\pi(n + \frac{1}{2})}\right)}, \qquad n \in \mathbb{N}. \quad (9)$$

The only undetermined parameter left is the width factor b, and since it is related to the flow field we can estimate it *a priori* by measuring the decrease of the midchannel velocity across the cross region:

$$b \approx \left\langle \frac{1}{V_{M,x}} \right\rangle_{x \in [-1,1], y=0} \approx 1.239, \quad (10)$$

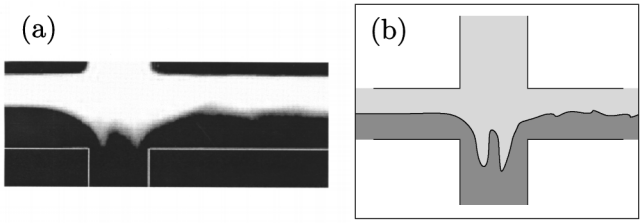

FIG. 5. Indication of an experimental second resonance state (a) compared to similar numerical state (b).

where $\langle \cdot \rangle$ denotes averaging in a range defined by the subscript.

The theoretical prediction of the resonances is shown in Fig. 4 as the thick solid curves. The theoretical model nicely captures the shape of the measured resonances, and despite the first two resonances a quantitative agreement is also found.

The experimental verification of the spatiotemporal resonances is still at an early stage, which excludes a quantitative comparison with the numerical/theoretical results. Still, indications of resonant states have been found experimentally, and are compared with the numerics in Fig. 5. The experimental microsystem was made in poly(dimethyl siloxane) (PDMS) using two-level soft lithography technology [15]. All channels are 200 μm wide and 26 μm high, and the solution consists of 46% glycerol and 54% water, where the upper part was been dyed by fluorescein in a 1 mM concentration. The mean flow rate through the main channel was 0.5 μL/min, and a more detailed description of the experiment is given in [16].

The resonances, which now have been observed numerically, indicated experimentally, and predicted theoretically, completely control the behavior of the mixer (i.e., the regions of strong and poor mixing in the parameter space), and from this information the optimal mixing configuration is achievable. This analysis, on the other hand, also gives the unexpected ability to use the mixer to enhance particle separation: The reason is that, when tuning the mixer at a resonance, the simple shape of the interface is unchanged, while the interfacial diffusion is enhanced due to the folding and subsequential unfolding of the interface. This effect is clearly seen in Fig. 5(a), where the interfacial diffusion on the right side is greatly enhanced compared to the left side. Finally, the original work of Taylor and more recent work of Dutta and Chevray [17] point out that diffusion across an interface plays an important role in particle separation. At present, particle separators working by diffusion exist [18], which will benefit directly from the mixer tuned at a resonance.

In conclusion we reveal, through numerical and theoretical work, the complete behavior and response of a simple micromixing system as a function of its two non-dimensionalized control parameters. The efficiency of mixing is strongly influenced by a resonance effect, which is observed experimentally, and arises due to an interplay between characteristic time scales and symmetries of the mixer. The good agreement between the predicted and measured resonances justifies the use of the simplified flow field in the estimation of T_A, and it especially supports the explanation of resonance, leading to the resonance relation Eq. (4).

We would like to thank Arash Dodge and Marie-Caroline Jullien from MMN-ESPCI for fruitful discussions and access to the experimental results.

[1] M. Wautelet, Eur. J. Phys. **22**, 601 (2001).
[2] K. D. Dorfman and H. Brenner, Phys. Rev. E **65**, 021103 (2002).
[3] H. Aref, J. Fluid Mech. **143**, 1 (1984).
[4] J. M. Ottino, *The Kinematics of Mixing: Stretching, Chaos, and Transport* (Cambridge University Press, Cambridge, England, 1989).
[5] Y.-K. Lee, C. Shih, P. Tabeling, and C. M. Ho, Proceedings of the MEMS2001, Interlaken, Switzerland, 2001, p. 483.
[6] M. Volpert, I. Mezic, C. Meinhart, and M. Dahleh, Proceedings of the ASME Mechanical Engineering International Congress and Exposition, Nashville, TN, 1999, p. 483.
[7] M. H. Oddy, J. G. Santiago, and J. C. Mikkelsen, Anal. Chem. **73**, 5822 (2001).
[8] Jr-H. Tsai and L. Lin, Sensors Actuators A **97–98**, 665 (2002).
[9] Abraham D. Stroock *et al.*, Science **295**, 647 (2002).
[10] R. H. Liu *et al.*, J. Microel. Syst. **9**, 190 (2000).
[11] We use a finite difference code in a vorticity/stream function formulation. In order to iteratively obtain the steady state velocity field, we use a quasitransient method similar to the work in [12]. Even though we use $\mathrm{Re} = 0.5 \neq 0$, we still treat the flow field as a solution to the creeping flow problem, i.e., superimposing the pure main and transverse flows in Eq. (2).
[12] G. Jilani, S. Jayaraj, and K. Khadar Voli, Heat Mass Transfer **38**, 261 (2002).
[13] IDL 5.5 from Research Systems (Kodac).
[14] We use this new method of interface analysis as the existing techniques (finite time Lyapunov exponents, etc.) fail to reveal the resonances seen in Fig. 4 because they relate to the full time evolution of the interface, while F depends only on the geometry of the end interface.
[15] M. Unger *et al.*, Science **288**, 113 (2000).
[16] A. Dodge *et al.*, Proceedings of μTAS 2003, Squaw Valley, California (2003), p. 935.
[17] P. Dutta and R. Chevray, Exp.Therm. Fluid Sci. **11**, 1 (1995).
[18] The H-Filter® Access™ Lab Card from Micromics, Canada.